

# Radial two-dimensional ion crystals in a linear Paul trap

Marissa D’Onofrio, Yuanheng Xie, A.J. Rasmusson, Evangeline Wolanski, Jiafeng Cui, and Philip Richerme<sup>1,2</sup>

<sup>1</sup>Indiana University Department of Physics, Bloomington, Indiana 47405, USA

<sup>2</sup>Indiana University Quantum Science and Engineering Center, Bloomington, Indiana 47405, USA

(Dated: May 25, 2022)

We present the first experimental study of radial two-dimensional ion crystals in a linear Paul trap. Using arrays of up to 19  $^{171}\text{Yb}^+$  ions, we create this two-dimensional crystal phase by imposing a large ratio of axial to radial trapping potentials. We demonstrate that the structural phase boundaries and vibrational mode frequencies of this crystal are well-described by a simple pseudopotential approximation, despite the time-dependent ion positions driven by intrinsic micromotion. We further observe that micromotion-induced heating of the radial two-dimensional crystal is confined to the radial plane. Finally, we verify that the transverse motional modes, which are used in most ion-trap quantum simulation schemes, remain decoupled and cold in this geometry. Our results establish radial two-dimensional ion crystals as a robust experimental platform for realizing a variety of theoretical proposals in quantum computation and simulation.

Laser-cooled ions in radio-frequency (rf) and Penning traps form Coulomb crystals, spatially ordered structures that arise due to a balance between trapping fields and Coulomb repulsion. Decades-long advancements in the preparation and control of cold ion crystals allow for precise manipulation of internal and external degrees of freedom [1], giving rise to applications spanning plasma physics [2, 3], high-precision spectroscopy [4, 5], cold molecules [6–8], and quantum computation [9–11] and simulation [12–15]. In these experiments, achieving the desired level of control has typically required an initial characterization of the ion positions, structural phases, normal mode frequencies, and sources of crystal heating.

Penning traps and rf (Paul) traps have long been the prevailing architectures for storing and manipulating ion Coulomb crystals. In both platforms, the structural and vibrational properties of the crystal are dictated by the aspect ratio  $\alpha \equiv \omega_z/\omega_r$  of the trap’s axial and radial secular frequencies. In Penning trap experiments, the full range of possible structural configurations has been observed and studied [16, 17], including the two-dimensional (2D) phase (at large  $\alpha$ ) where strong axial confinement squeezes ions into a single radial plane. This phase in particular has led to breakthroughs in validating cold Coulomb plasma theory and in simulating the quantum dynamics of interacting spin systems [18, 19].

In contrast, the corresponding radial 2D phase in linear Paul traps remains largely unexplored. To date, 2D ion crystals in rf traps have only been created using specialty electrode configurations [20, 21], in quasi-2D geometries at small  $\alpha$  [22–24], or in small systems of 3-4 ions [25]. Thus, many open questions remain about the structural stability, phase boundary, normal modes, and normal frequencies of large crystals in the radial 2D phase [26]. Moreover, it remains experimentally unknown the degree to which rf-driven micromotion could obscure site-specific imaging resolution or, even worse, lead to fast absorption of energy from the rf drive [27–29] and melting of the ion crystal [30].

In this Letter, we report the first characterization and coherent control of a radial 2D crystal in a linear Paul trap. We map the full range of structural phases for Coulomb crystals as a function of ion number using arrays of up to 19 ions, and we investigate the transverse vibrational mode spectrum in the radial 2D phase. Next, we measure the time-dependent temperature of the crystal as it experiences micromotion-induced heating, and we extract the center-of-mass heating rate along the micromotion-free direction perpendicular to the radial plane. Finally, we discuss the implications for future quantum information processing experiments.

Experiments are performed with  $^{171}\text{Yb}^+$  ions confined in a four-rod linear Paul trap with two “needle” endcaps along the axial direction ( $z$ -axis). Near the center of the trap, the time-dependent potential is written [31]

$$V(\vec{r}, t) = \frac{V_0 \cos(\Omega_t t)}{2r_0^2} (x^2 - y^2) + \frac{\kappa U_0}{2z_0^2} (2z^2 - x^2 - y^2) \quad (1)$$

where  $V_0$  and  $U_0$  are the rf and dc voltages,  $r_0 = 460 \mu\text{m}$  and  $z_0 = 335 \mu\text{m}$  are the radial and axial trap dimensions,  $\Omega_t = 2\pi \times 21 \text{ MHz}$  is the trap drive frequency, and  $\kappa$  is a geometric factor of order 1.

For low temperatures and weak axial confinement, the secular motion of an ion in a radially-symmetric trap is well-described by the 3D harmonic pseudopotential

$$\Phi(r, z) = \frac{1}{2} m \left( \omega_r^2 r^2 + \omega_z^2 z^2 \right) \quad (2)$$

where  $r^2 = x^2 + y^2$ , and the secular frequencies are

$$\omega_r = \sqrt{\frac{Q}{m} \left( \frac{qV_0}{4r_0^2} - \frac{\kappa U_0}{z_0^2} \right)}, \quad \omega_z = \sqrt{\frac{Q}{m} \frac{2\kappa U_0}{z_0^2}}. \quad (3)$$

Here  $Q$  is the ion charge,  $m$  the ion mass, and  $q = \frac{2QV_0}{mr_0^2\Omega_t^2}$  is the Mathieu “ $q$ ” parameter. In our experiments, we introduce a slight asymmetry between the  $x$  and  $y$  directions to prevent a zero-frequency rotational mode; here we choose  $\omega_r \equiv \text{Max}[\omega_x, \omega_y]$  for specificity.

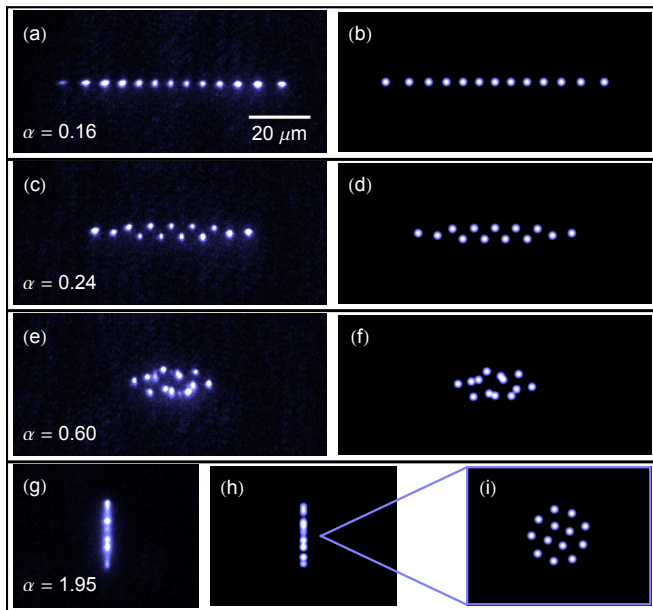


FIG. 1. Crystal configurations of 13 ions are shown for increasing values of the trap aspect ratio  $\alpha \equiv \omega_z/\omega_r$ . The structure transforms from a 1D chain (a, b) to zigzag (c, d) and 3D spheroidal phases (e, f), before ending in a 2D triangular lattice in the radial plane (g, h, i). Experimental ion positions (left) are in strong agreement with pseudopotential simulation results (right). Panel (h) includes first-order micromotion effects, as well as depth-of-field effects which slightly blur the Airy pattern of each ion. Panel (i) shows the same calculation as (h), rotated to better display the lattice structure.

*Structural Phase Transitions*—When the aspect ratio  $\alpha$  is small, ions form a 1D chain along the trap’s central axis and the pseudopotential approximation provides a high-accuracy description of ion positions and dynamics. In Figure 1(a), we show a 1D crystal of 13  $^{171}\text{Yb}^+$  ions, imaged by irradiating the  $369.5\text{ nm } ^2\text{S}_{1/2} \rightarrow ^2\text{P}_{1/2}$  transition and collecting fluorescence on an EMCCD camera. The ion positions are in excellent agreement with simulated results based on the pseudopotential approximation (Fig. 1(b)), for which the secular frequencies are determined by applying a resonant rf voltage to a nearby electrode [32].

As we raise  $\alpha$  (by increasing  $U_0$ ), the ions pass through a quasi-2D zig-zag phase (Fig. 1(c), (d)) and a number of 3D spheroidal configurations (Fig. 1(e), (f)), before forming a 2D crystal in the radial plane. This final configuration occurs in Fig. 1(g), (h), where the single plane of ions is viewed on-edge. (Fig. 1(i) shows the same crystal viewed perpendicularly to the plane.) In these higher- $\alpha$  phases, ions that lie away from the trap’s central axis are subject to rf-driven micromotion, the amplitude of which increases linearly with the ion’s radial coordinate. Though the equilibrium ion positions are no longer stationary due to micromotion, we nevertheless observe that the time-averaged positions correspond to predic-

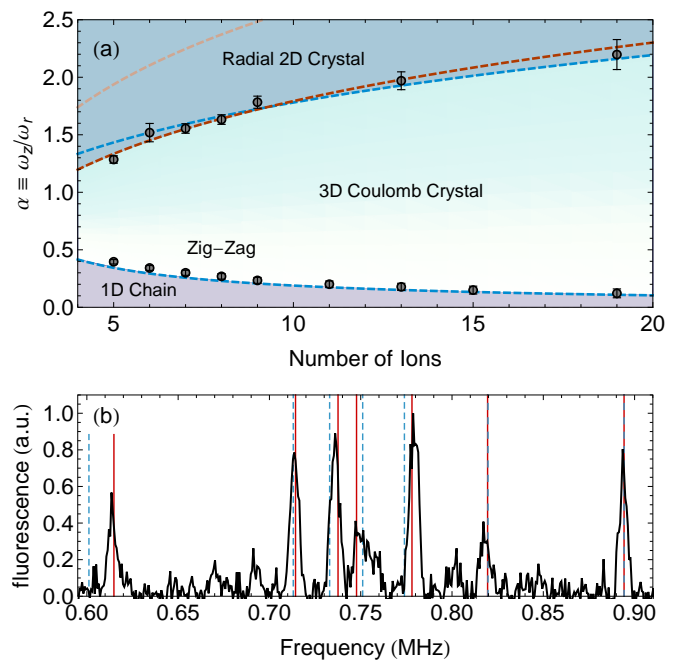


FIG. 2. (a) Phase diagram of ion Coulomb crystals in a linear Paul trap. Data show the measured  $\alpha$  that separate the 1D/zig-zag and 3D/radial 2D phases as a function of ion number. Three theory predictions (with no adjustable parameters) are plotted for comparison. Blue, pseudopotential [33]; Red, Floquet-Lyapunov [34]; Orange, micromotion-destabilized [35]. (b) Normal mode spectrum for 7 ions in a 2D crystal at  $\alpha = 2$ . Vertical lines show predicted mode frequencies. Blue, pseudopotential; Red, Floquet-Lyapunov.

tions obtained from pseudopotential theory calculations.

Varying the axial confinement over such a large range enables the precise experimental determination of structural phase transition boundaries at both small and large  $\alpha$ , as shown in Figure 2(a). Ions starting in a 1D chain exhibit a sudden transition to a zig-zag configuration at a critical value of  $\alpha$  that depends on particle number  $N$  [36]. Numeric estimates for small  $N$  predict a transition at  $\alpha = \frac{1}{.73N^{.86}}$  [37, 38], which has been previously verified in an experiment with up to 10 ions [39]. Our measurements confirm this power law behavior for up to 19 ions, plotted as the blue dashed line between the 1D and zig-zag phases in Fig 2(a).

For the 3D to radial 2D transition, different theoretical techniques currently provide different estimates of the phase boundary. Under the pseudopotential approximation, Dubin predicted that radial 2D crystals should form when  $\alpha = (2.264N)^{1/4}$  [33]. A separate analysis of the time-dependent potential has suggested the existence of a micromotion-destabilized region due to a downward shift in transverse mode frequencies, which would result in phase transitions at systematically larger  $\alpha$  [35]. A further time-dependent analysis using the Floquet-Lyapunov (FL) approach [34] shows much closer align-

ment with pseudopotential theory. Our measurements of the 3D to radial 2D phase boundary in Fig. 2(a) are consistent with both the pseudopotential and FL approaches (blue and red dashed lines, respectively) as opposed to the micromotion-destabilized theory (orange dashed line). For studies of radial 2D crystals, the absence of a micromotion-destabilized region greatly relaxes the constraints on trap parameters, while the close agreement with the pseudopotential approximation allows for a simplified physical understanding.

As a further investigation of micromotion effects, we measure the vibrational spectrum of a 7-ion crystal deep in the 2D regime. Global, far-detuned Raman transitions at 355 nm allow for spin-motion coupling and coherent excitation of the crystal modes [40]. The two Raman beams have a frequency difference near the  $^{171}\text{Yb}^+$  hyperfine ground state splitting  $\omega_{\text{hf}}$ , with the precise frequencies, amplitudes, and relative phases controlled by acousto-optic modulators [41]. In our experiment the transverse (drumhead) modes, which lie along the axial direction, are the most strongly excited since the wavevector difference of our Raman beams is aligned perpendicularly to the crystal plane.

The measured frequency spectrum following ion cooling and initialization is compared in Fig. 2(b) to normal mode frequencies calculated from standard pseudopotential theory (blue) and from the FL approach [34] (red). These methods largely agree with the measured data and with each other to within 2 kHz, though the pseudopotential approximation misses the lowest frequency mode by over 10 kHz. This discrepancy may prove unimportant for many experiments; for instance, in quantum simulations of spin-lattice Hamiltonians [15], the two methods would predict effective Ising interaction ranges that differ by only 1 part in  $10^3$ .

*Rf heating effects*—Even with a relatively unaltered mode structure, a small micromotion amplitude could still result in a strong effect on crystal lifetimes and temperatures. When multiple ions are confined in an rf trap, ion-ion interactions can transfer micromotion energy into secular kinetic energy and result in rapid rf heating [27, 28]. As the collision rate increases, ion motion becomes less correlated, and a sudden jump in temperature occurs at an inflection point which corresponds to a ‘melting’ of the crystal [30]. This rf heating mechanism is expected to dominate over other sources of noise, such as electric field fluctuations [42] and collisions with background gas molecules [29]. Though no prior experimental studies have probed the lifetime and heating rates of radial 2D crystals, molecular dynamics simulations indicate that 100+ ions could possibly be maintained for long times without continuous cooling [29].

To begin investigating the effects of micromotion-induced heating, we measure the trapping lifetimes of radial 2D crystals in the absence of active cooling. After the ions are Doppler cooled, the cooling beams are

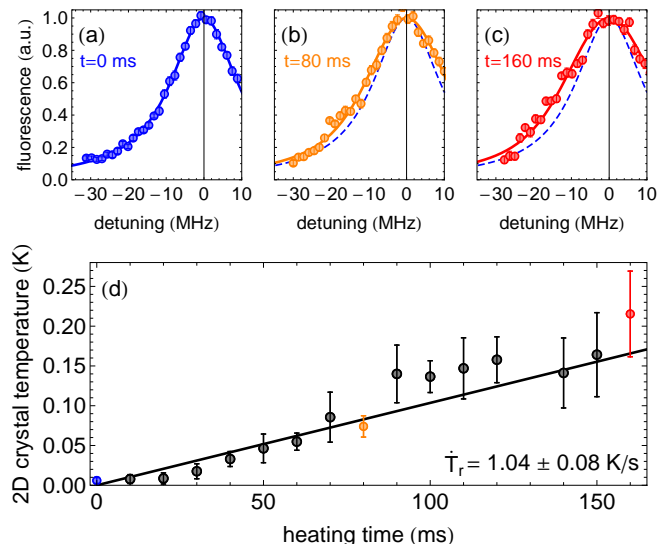


FIG. 3. Voigt fluorescence lineshapes of a 7 ion crystal exposed to rf heating are shown for heating times of (a) 0 ms, (b) 80 ms, and (c) 160 ms. The lineshape widens at later times due to increasing contributions from Doppler broadening. The 0 ms profile (3 mK temperature) is indicated by a dashed blue line in panels (b) and (c) for reference. (d) A radial heating rate of  $\dot{T}_r = 1.04 \pm 0.08$  K/s is extracted from Voigt profile fits to ion fluorescence data.

switched off and the ions are allowed to heat for a specified amount of time. If the crystal melts during this period, one or more ions may escape the trap confining potential or remain uncooled when the Doppler beams are re-applied. We measure the fraction of trials for which all ions remain in the crystal, and find that the  $1/e$  trapping lifetime is in excess of 5 seconds for up to 19 ions. This lifetime is exceptionally long compared to the typical  $\sim$ millisecond timescales of quantum computation or simulation experiments.

To further study rf heating effects, we determine the temperature of the radial 2D crystal by analyzing the ions’ fluorescence lineshape. The ion resonance, which is described by a Voigt distribution, is a convolution of Lorentzian and Gaussian profiles. The Lorentzian contribution comes from the power-broadened natural linewidth  $\Delta\nu_L = \Gamma\sqrt{1+s} = 2\pi \times 22$  MHz, where  $\Gamma = 2\pi \times 19.6$  MHz is the natural linewidth of the  $^{171}\text{Yb}^+$  369.5 nm transition and  $s = 0.3$  is the laser saturation parameter. The Gaussian contribution results from Doppler broadening, with a full-width at half-maximum of  $\Delta\nu_G = 2\sqrt{\frac{(2\ln 2)k_B}{m\lambda^2}} \sqrt{T_r \cos^2 \theta + T_z \sin^2 \theta}$ . This expression arises since our fluorescence beam intersects the crystal plane at an angle ( $\theta = 45^\circ$ ) and is therefore sensitive to both the radial and axial temperatures  $T_r$  and  $T_z$ . Later we will show that keeping independent radial and axial temperatures is well-justified, and that the axial temperature adds negligible contribution to the overall

linewidth.

To extract the radial crystal temperature, we fit the measured Voigt fluorescence profile to a Lorentzian of constant width  $\Delta\nu_L$  and a Gaussian of variable width  $\Delta\nu_G$ . When the crystal is Doppler cooled to 3 mK (as confirmed with sideband Raman spectroscopy), the Gaussian contribution is small and the line profile is essentially Lorentzian (Fig. 3(a)). However, if the cooling beams are extinguished and the crystal acquires radial energy through rf heating, the fluorescence profile spreads due to an increase in thermal motion (Fig. 3(b,c)). By performing many temperature measurements at increasing heating times, as shown in Fig. 3(d), we determined the radial heating rate to be  $\dot{T}_r = 1.04 \pm .08$  K/s. Previous work has predicted non-linear heating near the melting point of Coulomb crystals; the linear nature of our data implies that short time scales, large ion masses, and low initial temperatures keep crystals far from this limit [28, 30].

In the above analysis, we have assumed that the overall crystal temperature is dominated by the radial component  $T_r$  and that the radial and axial temperatures remain unequilibrated. This can be qualitatively understood as rf heating effects arise from micromotion in the radial plane, thus heat transfer between radial and axial modes should be strongly suppressed in the radial 2D geometry. We further support this assumption by performing a molecular dynamics simulation of ions in small 2D and 3D crystal configurations (following [28]), finding that only the 3D crystals show significant heating. If true, this would be especially relevant to quantum information experiments, where cold, isolated phonon modes are prerequisites for performing high-fidelity quantum operations [15, 43]. Nevertheless, experimental imperfections such as trap anharmonicities and misalignments have the potential to cross-couple radial energy into the transverse modes and catalyze significant axial heating.

To look for evidence of heat transfer between the radial and axial directions, we measure the heating rate of the axial center-of-mass (COM) mode using resolved sideband spectroscopy. Following Doppler cooling, our 355 nm Raman beams are used to sideband cool the axial COM mode to  $\bar{n} \lesssim 2.5$  as well as to induce stimulated Raman transitions at the axial COM red and blue sideband frequencies,  $\omega_{\text{hf}} \pm \omega_z$ . Coherent oscillations of these sidebands result in profiles like those shown in Fig. 4(a), which are performed on a radial 2D crystal of 7 ions immediately after sideband cooling.

The number of quanta in the axial COM mode is determined by taking the ratio  $r$  of red to blue sideband transition probability amplitudes for several different sideband drive times. For a thermal distribution of harmonic oscillator levels, the mean occupation number is then given by  $\bar{n} = \frac{r}{1-r}$ . Finally, the axial COM heating rate  $\dot{\bar{n}}$  is determined by leaving the crystal uncooled for increasing time periods and repeating the sideband measurements.

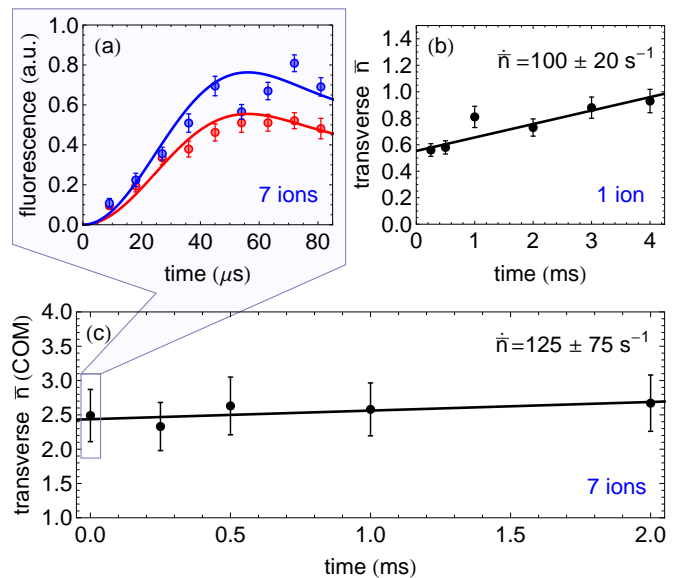


FIG. 4. (a) A comparison of red and blue sideband probability amplitudes are shown for a 7 ion crystal immediately following sideband cooling. The heating rate of the transverse (axial) COM mode for a single ion (b) is comparable to that of a 7 ion crystal (c). In both cases, the heating rate is low compared to other traps of similar dimension.

We first assess the axial COM heating rate for a single ion at the center of our trap, with  $\omega_z \approx 2\pi \times 900$  kHz and a relatively large  $\alpha = 2$ . This determines our trap's intrinsic heating rate due to electric field noise, since the single ion is undriven by micromotion. As shown in Fig. 4(b), we find a heating rate of  $\dot{\bar{n}} = 100 \pm 20$  motional quanta/s. This rate, which corresponds to temperature heating rate  $\dot{T}_z = 0.004 \pm 0.001$  K/s and a spectral density of electric field noise  $S_E = 2.65 \times 10^{-12} \text{ V}^2 \text{ m}^{-2} \text{ Hz}^{-1}$ , compares favorably to the heating rates measured in other room-temperature rf traps of similar size [42].

Using the same trap parameters as above ( $\omega_z \approx 2\pi \times 900$  kHz and  $\alpha = 2$ ), we repeat the heating rate measurements for a radial 2D crystal of 7 ions. As shown in Fig 4(c), a linear fit yields the measured heating rate  $\dot{\bar{n}} = 125 \pm 75$  quanta/sec. In temperature units, this rate is over 200 times smaller than the measured radial heating (Fig. 3) and justifies our earlier assumption of non-equilibration between axial and radial directions. Furthermore, the comparable heating rates for 1 and 7 ions strongly indicate that radial micromotion does not couple to the transverse direction and suggest that noise sources in our trap are largely uncorrelated [42]. Our observations confirm that the transverse (drumhead) modes of our radial 2D crystal remain isolated and cold, and that rapid rf heating mechanisms are confined to the radial plane.

*Discussion and Outlook*—Prior to this work, it was experimentally unknown whether micromotion in a linear Paul trap would lead to destabilized trapping re-

gions, altered normal mode frequencies, impractically short lifetimes, or fast rf-driven heating. We find that micromotion effects are largely constrained to the radial plane: the phase boundaries and vibrational spectra are well-predicted by micromotion-free pseudopotential theory, and only the radial degrees of freedom experience micromotion-induced heating. In contrast, the axial degrees of freedom remain decoupled and cold.

Our demonstration of stable, isolated, and low-noise transverse modes establishes radial 2D crystals in linear Paul traps as a realistic platform for implementing several quantum simulation and computation proposals [20, 26, 35, 44]. For instance, radial 2D crystals in rf traps form stable triangular lattices and are especially well-suited for studies of highly-frustrated quantum magnets [26, 45]. Such exotic materials are known to have rich phase diagrams and may be a mechanism underlying high- $T_C$  superconductivity [46], but to date are still poorly understood [47]. Radial 2D ion crystals could also provide an alternative solution for fault-tolerant quantum computing, since the 2D geometry can hold larger numbers of qubits more efficiently than 1D strings, with a higher error threshold for fault-tolerance [35, 44]. Additionally, 2D ion arrays can simplify preparations for one-way quantum computing schemes, in which 2D cluster states can be used to simulate any quantum circuit. [48, 49]. The ability to control and probe radial 2D Coulomb crystals in a linear Paul trap offers a robust experimental system for investigating open questions in many-body physics and new opportunities for realizing large-scale quantum computation.

This work was supported by the U.S. Department of Energy, Office of Science, Basic Energy Sciences, under Award #DE-SC002034. The IU Quantum Science and Engineering Center is supported by the Office of the IU Bloomington Vice Provost for Research through its Emerging Areas of Research program.

- 
- [1] M. Drewsen, *Physica B: Condensed Matter* **460**, 105 (2015).
  - [2] J. Malmberg and J. DeGrassie, *Physical Review Letters* **35**, 577 (1975).
  - [3] D. H. Dubin and T. O’Neil, *Reviews of Modern Physics* **71**, 87 (1999).
  - [4] C.-w. Chou, D. Hume, J. Koelemeij, D. J. Wineland, and T. Rosenband, *Physical Review Letters* **104**, 070802 (2010).
  - [5] H. A. Füst, C.-H. Yeh, D. Kalincev, A. P. Kulosa, L. S. Dreissen, R. Lange, E. Benkler, N. Huntemann, E. Peik, and T. E. Mehlstäubler, *Physical Review Letters* **125**, 163001 (2020).
  - [6] K. Mølhave and M. Drewsen, *Physical Review A* **62**, 011401 (2000).
  - [7] W. G. Rellergert, S. T. Sullivan, S. Kotochigova, A. Petrov, K. Chen, S. J. Schowalter, and E. R. Hudson, *Physical Review Letters* **107**, 243201 (2011).
  - [8] C.-Y. Lien, C. M. Seck, Y.-W. Lin, J. H. Nguyen, D. A. Tabor, and B. C. Odom, *Nature Communications* **5**, 1 (2014).
  - [9] K. R. Brown, J. Kim, and C. Monroe, *Nature Quantum Information* **2**, 1 (2016).
  - [10] J. P. Gaebler *et al.*, *Physical Review Letters* **117**, 060505 (2016).
  - [11] K. Wright *et al.*, *Nature Communications* **10**, 1 (2019).
  - [12] A. Friedenauer, H. Schmitz, J. T. Glueckert, D. Porras, and T. Schätz, *Nature Physics* **4**, 757 (2008).
  - [13] P. Richerme, Z.-X. Gong, A. Lee, C. Senko, J. Smith, M. Foss-Feig, S. Michalakis, A. V. Gorshkov, and C. Monroe, *Nature* **511**, 198 (2014).
  - [14] P. Jurcevic, B. P. Lanyon, P. Hauke, C. Hempel, P. Zoller, R. Blatt, and C. F. Roos, *Nature* **511**, 202 (2014).
  - [15] C. Monroe *et al.*, arXiv preprint arXiv:1912.07845 (2019).
  - [16] S. Gilbert, J. Bollinger, and D. Wineland, *Physical Review Letters* **60**, 2022 (1988).
  - [17] S. Mavadia, J. F. Goodwin, G. Stutter, S. Bharadia, D. R. Crick, D. M. Segal, and R. C. Thompson, *Nature Communications* **4**, 1 (2013).
  - [18] T. Mitchell, J. Bollinger, D. Dubin, X.-P. Huang, W. Itano, and R. Baughman, *Science* **282**, 1290 (1998).
  - [19] J. W. Britton, B. C. Sawyer, A. C. Keith, C.-C. J. Wang, J. K. Freericks, H. Uys, M. J. Biercuk, and J. J. Bollinger, *Nature* **484**, 489 (2012).
  - [20] B. Yoshimura, M. Stork, D. Dadić, W. C. Campbell, and J. K. Freericks, *EPJ Quantum Technology* **2**, 2 (2015).
  - [21] M. Ivory, A. Kato, A. Hasanzadeh, and B. Blinov, *Review of Scientific Instruments* **91**, 053201 (2020).
  - [22] M. Block, A. Drakoudis, H. Leuthner, P. Seibert, and G. Werth, *Journal of Physics B: Atomic, Molecular and Optical Physics* **33**, L375 (2000).
  - [23] L. Yan, W. Wan, L. Chen, F. Zhou, S. Gong, X. Tong, and M. Feng, *Scientific reports* **6**, 21547 (2016).
  - [24] Y. Wang *et al.*, *Advanced Quantum Technologies* **3**, 2000068 (2020).
  - [25] H. Kaufmann, S. Ulm, G. Jacob, U. Poschinger, H. Landa, A. Retzker, M. Plenio, and F. Schmidt-Kaler, *Physical Review Letters* **109**, 263003 (2012).
  - [26] P. Richerme, *Physical Review A* **94**, 032320 (2016).
  - [27] V. L. Ryjkov, X. Zhao, and H. A. Schuessler, *Physical Review A* **71**, 033414 (2005).
  - [28] C. B. Zhang, D. Offenber, B. Roth, M. Wilson, and S. Schiller, *Physical Review A* **76**, 012719 (2007).
  - [29] I. Buluta, M. Kitaoka, S. Georgescu, and S. Hasegawa, *Physical Review A* **77**, 062320 (2008).
  - [30] K. Chen, S. T. Sullivan, W. G. Rellergert, and E. R. Hudson, *Physical Review Letters* **110**, 173003 (2013).
  - [31] D. J. Wineland, C. Monroe, W. M. Itano, D. Leibfried, B. E. King, and D. M. Meekhof, *Journal of Research of the National Institute of Standards and Technology* **103**, 259 (1998).
  - [32] H. Nägerl, D. Leibfried, F. Schmidt-Kaler, J. Eschner, and R. Blatt, *Optics Express* **3**, 89 (1998).
  - [33] D. H. Dubin, *Physical Review Letters* **71**, 2753 (1993).
  - [34] H. Landa, M. Drewsen, B. Reznik, and A. Retzker, *New Journal of Physics* **14**, 093023 (2012).
  - [35] S.-T. Wang, C. Shen, and L.-M. Duan, *Scientific reports* **5**, 8555 (2015).
  - [36] The 1D to zig-zag transition only occurs due to non-degenerate radial frequencies and is quite close to the un-

- mapped zig-zag to 3D boundary for our near-degenerate trap. Numerous unmapped subtransitions occur within the 3D Coulomb crystal phase; the richness of 3D geometries that arises with even 3-4 ions is detailed in [25].
- [37] J. Schiffer, *Physical Review Letters* **70**, 818 (1993).
  - [38] A. Steane, *Applied Physics B* **64**, 623 (1997).
  - [39] D. Enzer *et al.*, *Physical Review Letters* **85**, 2466 (2000).
  - [40] W. Campbell, J. Mizrahi, Q. Quraishi, C. Senko, D. Hayes, D. Hucul, D. Matsukevich, P. Maunz, and C. Monroe, *Physical Review Letters* **105**, 090502 (2010).
  - [41] R. Islam, C. Senko, W. Campbell, S. Korenblit, J. Smith, A. Lee, E. Edwards, C.-C. Wang, J. Freericks, and C. Monroe, *science* **340**, 583 (2013).
  - [42] M. Brownnutt, M. Kumph, P. Rabl, and R. Blatt, *Reviews of modern Physics* **87**, 1419 (2015).
  - [43] C. Ballance, T. Harty, N. Linke, M. Sepiol, and D. Lucas, *Physical Review Letters* **117**, 060504 (2016).
  - [44] C. Shen and L.-M. Duan, *Physical Review A* **90**, 022332 (2014).
  - [45] L. Balents, *Nature* **464**, 199 (2010).
  - [46] P. W. Anderson, *science* **235**, 1196 (1987).
  - [47] H. T. Diep, *Magnetic systems with competing interactions: frustrated spin systems* (World Scientific, AD-DRESS, 1994).
  - [48] R. Raussendorf and H. J. Briegel, *Physical Review Letters* **86**, 5188 (2001).
  - [49] H. Wunderlich, C. Wunderlich, K. Singer, and F. Schmidt-Kaler, *Physical Review A* **79**, 052324 (2009).